THE JOURNAL OF PHYSICAL CHEMISTRY C

Article

pubs.acs.org/JPCC

Kinetic Trapping of D_2 in MIL-53(Al) Observed Using Neutron Scattering

Rachel A. Pollock,[†,‡] Jae-Hyuk Her,[†,‡,⊥] Craig M. Brown,[*,†,§] Yun Liu,[†,§] and Anne Dailly[∥]

[†]NIST Center for Neutron Research, National Institute of Standards and Technology, Gaithersburg, Maryland 20899, United States

[‡]Department of Materials Science and Engineering, University of Maryland, College Park, Maryland 20742, United States

[§]Department of Chemical Engineering, University of Delaware, Newark, Delaware 19716, United States

[∥]Global Research & Development, General Motors, Warren, Michigan 48090, United States

Supporting Information

ABSTRACT: We have studied gas adsorption effects on the structure of a metal−organic framework, MIL-53(Al), a material well-known because of the controllable framework "breathing" phenomenon. Neutron powder diffraction between 4 and 77 K and up to 4.5 bar pressure D_2 confirms that a structural phase transition is responsible for the observed H_2/D_2 isotherm hysteresis at 77 K. We find two crystallographically distinct D_2 adsorption sites in MIL-53(Al) when the pores are fully opened, similar to those reported for D_2 in MIL-53(Cr), but in contrast with the previously published cases of CO_2 and H_2O. Upon desorption of D_2 at 77 K, we find strong evidence for the existence of D_2 molecules kinetically trapped in the center of the closed pore of MIL-53(Al). This "molecular clamp" appears to be functional until ≈120 K, the temperature at which the D_2 eventually desorbs under dynamic vacuum. Hydrogen diffusion constants calculated using quasielastic neutron scattering data collected along the isotherm are also consistent with H_2 being trapped in the closed pore structure. Diffraction experiments performed with N_2 and He gases under similar conditions show the range of structural response from immediate pore opening at low N_2 pressures (<1 bar) to no observable effect at 10 bar He.

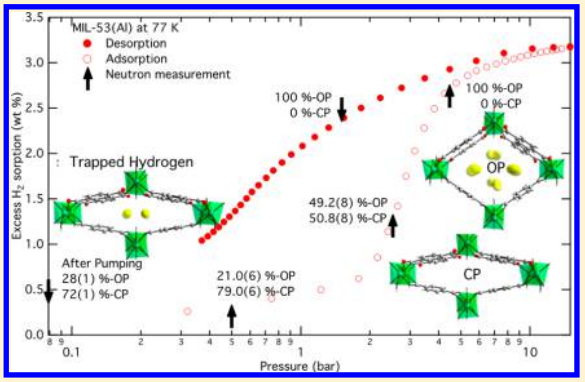

INTRODUCTION

The variety of chemical structures and functionalities displayed upon connecting metallic species to one another through organic ligands to yield porous, crystalline materials known as metal−organic frameworks (MOFs) has resulted in a booming research arena. The ability to tune the respective components, altering the structure and porosity, along with the subsequent impact on host−guest properties,[1−7] makes these materials interesting for potential applications such as hydrogen storage,[8−13] methane storage,[14−17] carbon dioxide capture,[18−21] industrial separations,[1−7,22−31] sensors,[8−10,32,33] drug-delivery,[14−17,34] and heterogeneous catalysis.[18−20,35−37]

A particular family of MOFs, known as MIL-53s, were some of the first materials to exhibit a large framework "breathing" phenomenon characterized by unit-cell volume changes of around 40%,[38] though several more examples exist.[39−48] This characteristic framework flexibility has been observed in MIL-53 upon loading guest molecules or changing temperature and/or pressure and has an associated large hysteresis.[49,50] It has also been shown that the adsorption and desorption history of a MIL-53(Al) sample plays a significant role in its structural transitions.[51] Additionally, it is well-known that polar molecules, such as H_2O and CO_2, loaded into the MOF induce the collapse of the open MIL-53 structure and locate in the center of the closed pore (CP);[52,53] however, even the noble gas Xe can induce the same effect.[54] The material also exhibits gas selectivity for CO_2 over nonpolar CH_4,[52] especially when the system is hydrated[55] or functionalized.[56] Upon chemical functionalization of the ligands, the overall structural motif is retained because of the inherent flexibility of the framework.[57] Further, this breathing phenomenon is also dependent on cation choice[1,58,59] with some control being exerted through cation mixing; the pore opening in a mixed Cr/Fe system is intermediate between the "easy" to open Cr and the harder to open Fe.[60] These interesting properties encouraged significant effort in both theoretical and experimental approaches to understanding the adsorption mechanisms and associated breathing phenomena with external stimuli[49,50] or with adsorbents, including CO_2,[61−65] C_nH_{2n+2},[66−69] and H_2 molecules,[70−73] among others.[74−77]

Structurally, MIL-53 is composed of corner-sharing metal clusters interconnected with benzenedicarboxylate (BDC) organic ligands. Upon removal of solvent molecules by evacuating the sample at moderate temperatures, MIL-53(Al)

Received: May 17, 2014
Revised: June 13, 2014
Published: July 14, 2014

   dx.doi.org/10.1021/jp504870n | J. Phys. Chem. C 2014, 118, 18197−18206

has a large, open pore (OP) structure (high temperature (HT) phase; space group *Imma*). The narrow, closed pore (CP) form that can be arrived at by cooling MIL-53(Al) is monoclinic with reduced pore volume (low temperature (LT) phase; space group $C2/c$). In this CP phase, the accordion-like compression of the unit cell geometry is accompanied by a twisting of both the BDC ligands and distortions of the metal−oxygen octahedra.[50]

A combination of temperature-dependent diffraction, inelastic neutron scattering, and density functional theory (DFT) calculations have been used to understand hydrogen adsorption in MIL-53(Cr).[78] The diffraction data taken at 10 K were used to define four separate adsorption sites for hydrogen, while the isobaric (2 bar) temperature-dependent data revealed the occupancy dependence of each of these sites and an approximate 2% change in unit cell volume upon hydrogen desorption at temperatures above 20 K. All the data were analyzed within the *Imcm* space group (pristine unit cell parameters: a = 16.772 Å, b = 13.145 Å, c = 6.847 Å), and unlike MIL-53(Al), the Cr-variety does not apparently exhibit a transition to the LT/CP phase on simply being cooled.[78]

In this paper, we report a quantitative multiphase structural analysis of the breathing effect in MIL-53(Al) using neutron powder diffraction (NPD) while performing an in situ isotherm measurement at 77 K. To further investigate the guest−framework interactions, we complement D_2 isotherm measurements with NPD measurements of nitrogen (N_2) and helium (He) at various temperatures and pressures. The latter gives context to surface area measurments that typically use He as a correction factor and N_2 for the surface area measurement. Quasielastic neutron scattering (QENS) data were also collected to study the dynamics of hydrogen in the MIL-53(Al) framework following the isotherm hysteresis at 77 K. These novel measurements yield rich structural information as a function of gas type, temperature, and pressure.

EXPERIMENTAL SECTION

The MIL-53(Al) used for these experiments was the same as that used for our previous neutron studies[50] and was synthesized according to literature preparation methods.[53,70] Briefly, the sample was prepared by hydrothermal reaction between the nitrate salt of the metal ion ($Al(NO_3)_3{\cdot}9H_2O$) and terephthalic acid (1,4-benzenedicarboxylic acid, H_2BDC) in a Teflon-lined stainless steel Parr bomb. (Certain trade names and company products are mentioned in this paper to adequately specify the experimental procedure and equipment used. In no case does this imply recommendation or endorsement by NIST, nor does it imply that the products are necessarily the best available for this purpose.) The as-synthesized powders were then rinsed with deionized water. Further activation treatments were performed on the as-synthesized materials to remove the unreacted acid located outside and within the pores. Free terephthalic acid filling the pores of the as-synthesized MIL-53(Al) was removed by calcination.

Neutron data were collected at the National Institute of Standards and Technology (NIST) Center for Neutron Research (NCNR); NPD data were collected using the BT-1 high-resolution powder diffractometer, while QENS data were collected using the disk chopper spectrometer (DCS).[79] For all neutron experiments, the dehydrated sample was degassed using a turbomolecular pump at a temperature of 120 °C overnight (to ensure all the sample is in the HT phase); the sample was then transferred into a sample cell which was fitted with a stainless steel gas dosing line and sealed with an indium O-ring in a He glovebox. Any adsorbed He gas was pumped out using a turbomolecular vacuum pump when the sample cell was mounted to the sample stick. A top-loading closed-cycle refrigerator was used to control the sample temperature with a temperature sensor mounted directly above the sample cell. A volumetric system was used to dose known quantities of gas or apply a certain equilibrium pressure depending on the measurement.

NPD data were collected using a Ge(311) monochromator with an in-pile 15′ collimation corresponding to a neutron wavelength (λ) of 2.0787(2) Å and 664 mg MIL-53(Al) sample. For dihydrogen NPD experiments, we used deuterium (D_2) gas because the incoherent scattering from H_2 results in a significant background in the data. D_2 and He gases were loaded into the MIL-53(Al) sample can at 77 K, while N_2 was loaded at 80 K. A vanadium cell was used to collect NPD data for gas-loading experiments with cell pressures under 1 bar, while a thicker-walled aluminum cell was used for pressure experiments up to 10 bar. Vanadium does not produce any significant Bragg peaks; Bragg peaks are observable when using aluminum, but they appear at known positions and can be removed from the diffraction pattern before analysis.

Rietveld refinements were performed using the computer program TOPAS-Academic[80] with structure models exploiting rigid body descriptions for the BDC ligands to reduce the number of total parameters to refine. The powder patterns in the LT/CP phase show anomalous line shapes with strong anisotropic broadening effects evident in the peak profile as a function of Miller indices (hkl), which was incorporated in the Rietveld analysis procedure.[81] The anomalous line shapes are observed only in nonzero k reflections of the narrow CP phase, implying that the lattice parameter along the largest breathing direction has a distribution of values, though higher-resolution data would be needed to better determine the exact distributions.

For QENS measurements, the DCS spectrometer was operated in low-resolution mode with an incident neutron wavelength of 6.0 Å, providing a full-width at half-maximum (fwhm) resolution of ca. 70 μeV at the elastic channel with an available momentum transfer (Q) range of 0.27−1.78 Å^{-1}. A cylindrical aluminum sample can 10 cm tall with a diameter of 1.2 cm was used, and 562.5 mg MIL-53(Al) was placed in a foil packet creating an annular geometry in the sample can. H_2 gas was loaded into the MIL-53(Al) sample can at 77 K, and QENS spectra were collected. Standard corrections were made, and the bare data was subtracted from each gas-loaded spectrum measured to generate the scattering function, $S(Q,\omega)$. The DAVE software package was used for data reduction and peak fitting.[82] More details about the QENS data reduction are presented in the Supporting Information.

RESULTS AND DISCUSSION

D_2 Adsorption. Because both the gas adsorption and NPD measurements were performed at cryogenic temperatures (≤80 K), we must keep in mind the large thermally driven pore-closing and opening hysteresis which was previously described (HT → LT, ca. 138 K and LT → HT, ca. 350 K, respectively) results in a mixed phase system, in which at 77 K the LT phase is predominately observed (88%; space group $C2/c$).[50] To identify possible sites at 77 K, we initially loaded D_2 gas at 77 K and cooled to 4 K to measure the NPD patterns, as the thermal

motion of the molecules would be at a minimum. Using the relative intensities of the Bragg peaks at ≈18° and ≈20° as a crude measure of the identity of the phase fractions, we again observed two phases for D_2 loadings from 0.5 D_2/Al to 3.0 D_2/Al (Figure S1 of the Supporting Information). However, the details of the structures are not the same as for the bare MIL-53(Al). Rather than displaying Bragg peaks consistent with the HT and LT phases within the *Imma* and *C*2/*c* space groups, respectively, we were unable to index the OP phase with orthorhombic symmetry. We determined that for all D_2 loadings the OP phase is slightly compressed, causing the benzene rings to be slightly canted, resulting in a distinct OP, monoclinic phase compatible with the *C*2/*c* space group, similar to that observed with organic adsorbates;[75] we will refer to this as the OP-D_2 phase.

Rietveld refinement of the D_2 loaded MIL-53(Al) NPD data is well-described using the aforementioned structure model (Figures S2−S5 and Tables S1−S9 of the Supporting Information). The adsorbed phases are described by an OP-D_2 phase and a coexisting CP phase, incorporating the adsorbed D_2 modeled as quantum rotationally, spherically averaged molecules with double occupancy of a deuterium atom.[83] At low temperature, the MIL-53(Al) dominantly forms the CP structure. As the amount of D_2 loaded into the sample increases, the amount of the OP-D_2 phase also increases (from 15.9 wt % at 0.5 D_2/Al to 79.4 wt % at 3.0 D_2/Al). In the loading range experimentally covered, the two phases always coexist. There is a relatively large uncertainty in the deuterium occupancies in the lower loading cases, with a strong correlation between the atom displacement parameter and occupancy, necessitating the fixing of one of the parameters to obtain stable and chemically meaningful refinements. Releasing both parameters in the refinement allocates more than one D_2 molecule per Al, an unphysical situation; hence, in these cases we fixed the maximum D_2 occupation to equal that experimentally dosed.

The Fourier difference map of the 3.0 D_2/Al loading shows two regions of excess nuclear scattering that can be attributed to the adsorption sites for D_2 (Figure 1); one site (D1) is close to the benzene ring (≈ 3.3 Å) of the BDC ligand while the remaining three sites are closer to the AlO_6 clusters. The three remaining sites are in close contact such that they cannot be occupied at the same time. For the highest loading measured, the D3 site is closest to two different oxygen atoms and is evidently stabilized the most, leading to a higher occupation at that site (0.58(3) D_2) and less at the others (0.35(3) D_2). As the phase fraction in the total pattern was reduced for the lower loadings, the refinements were less stable and an occupancy constraint was applied to make sites D2 and D4 be equal. To be consistent this was also applied to the 3.0 loading. Structurally, the response of MIL-53(Al) to the loading of D_2 is quite different from that observed for polar molecules like H_2O or CO_2. First, there are no D_2 molecules observed in the narrow/CP phase, only in the OP phase. Second, adsorbing D_2 does not induce a collapse of the pore structure as seen when polar molecules are adsorbed, but rather induces a greater phase fraction of the OP structure.

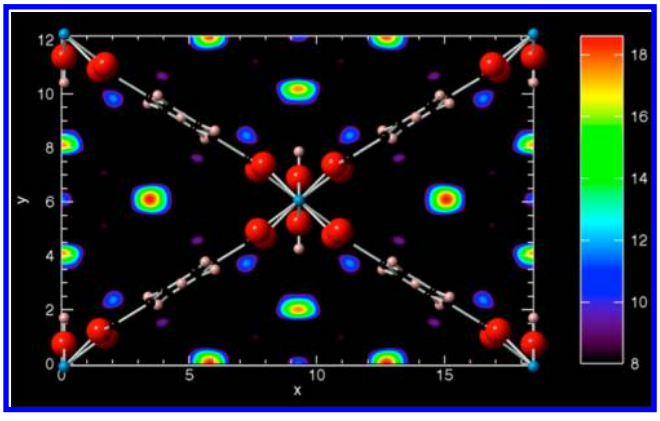

Figure 1. Fourier difference map of 3.0 D_2/Al loaded at 77 K and measured at 4 K in MIL-53(Al). Colors represent neutron scattering length densities of D_2 imaged down the *c*-axis, with the atomic structure of MIL-53(Al) superimposed for positional clarity.

D_2 Isotherm Measurements at 77 K. Following the gas adsorption isotherm with pressurized D_2 experiments at 77 K is more relevant in practice to further understanding the nature of the adsorption isotherm hysteresis through structural changes. After the MIL-53(Al) sample in the Al can (described above) was cooled to 77 K, D_2 gas was applied progressively from 0.5 to 4.5 bar (adsorption branch) and subsequently reduced to 1.5 bar (desorption branch). NPD data were collected at 77 K for these loadings and additional patterns were collected (measured at 77 K) after a vacuum was applied for 30 min at 77, 100, and 120 K (Figure 2). Pressures for which the NPD measurements were collected along the H_2 isotherm are presented in Figure S6 of the Supporting Information. The diffraction patterns observed at lower pressure (ca. 0.5−2.5 bar) have two phases, both OP-D_2 and CP, while for higher pressure (4.5 bar) and measurement along the desorption branch (1.5 bar), NPD data showed only a single OP-D_2 phase (Table S10 of the Supporting Information). The description of the evacuated-D_2 case will be discussed in the subsequent section.

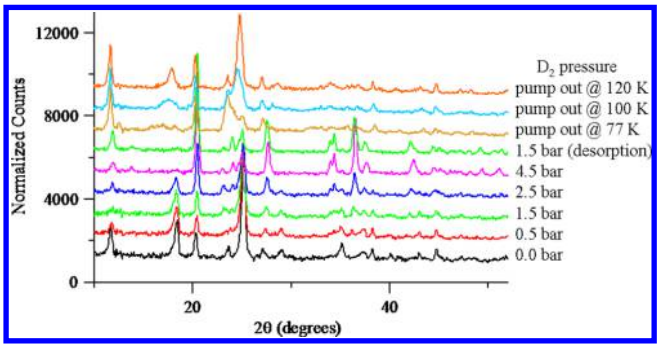

Figure 2. NPD patterns of MIL-53(Al) measured from 0.5 to 4.5 bar (increasing pressure) D_2 and 1.5 bar (decreasing pressure) D_2 at 77 K and after pumping out for about 30 min at 77, 100, and 120 K. The full patterns up to $2\theta = 110°$ are given in Figure S5 of the Supporting Information.

D_2 locations were determined by applying the simulated annealing (SA) method combined with the structural information determined in the preliminary D_2 loading experiments at 4 K. SA was used because the adsorbed D_2 was more disordered at the higher temperature of 77 K and therefore more difficult to unambiguously locate through Fourier difference mapping. Because we know that only the monoclinic *C*2/*c* OP structure will adsorb the D_2, all structural parameters defining the framework structure of MIL-53(Al) are fixed at their low-temperature values and the D_2 molecule(s) was added in the OP structure model where its position, occupancy, and

dx.doi.org/10.1021/jp504870n | J. Phys. Chem. C 2014, 118, 18197−18206

anisotropic displacement parameter (ADP) were allowed to vary. For 0.5 bar D_2, several independent SA runs commonly suggested that only the first site, the benzene ring position, is occupied with adsorbed D_2. The refined structure model for the lowest pressure is presented in Figure 3a (see the Rietveld refinement, Figure S8, and crystallographic data, Tables S11 and S12, in the Supporting Information). There is no clear experimental evidence that the second D_2 site, neighboring Al–O_6 cluster, was occupied until 2.5 bar D_2 was applied (Rietveld analysis and refined structure, Figures S10 and S11, respectively, and crystallographic data, Tables S13 and S14 of the Supporting Information). However, this does preclude that the second site is not occupied at lower pressure because it could be so highly disordered along the channel direction that its associated scattering density is lower than the detection limit of the current NPD experiment and modeling procedure.

Above 2.5 bar D_2, attempts to use the structural model with only one D_2 molecule could not satisfactorily explain the observed NPD pattern of OP phase regardless of the number of SA trials attempted. The second D_2 site was observed in the NPD data and was determined by SA to be similar to the second site observed in the 3.0 D_2/Al loading data at 4 K. At the highest pressure, 4.5 bar D_2, the CP phase has completely disappeared and all the MIL-53(Al) sample has transformed into the OP-D_2 structure (Rietveld fit, Figure S12, and crystallographic data, Table S15, in the Supporting Information). The quality of the single-phase NPD data allowed us to refine the ADPs of adsorbed D_2 molecules whose structure is presented in Figure 3b. The large ADP parameter indicates that the D_2 located at the second adsorption site is disordered along the pore channel. There is evidently significant disorder here as the 3 different adsorption sites identified at low temperatures could not be observed, and we considered only one site in the remaining 77 K analysis. To investigate the isotherm hysteresis, we reduced the pressure from 4.5 to 1.5 bar and the resulting structure did not return to the two-phase system observed during D_2 adsorption at 1.5 bar (Rietveld analysis, Figure S13 of the Supporting Information). The MIL-53(Al) structure still retained the single phase, OP-D_2 structure with D_2 molecules adsorbed, although the second D_2 adsorption site is more delocalized than that at 4.5 bar (Figure S14 of the Supporting Information).

These structural observations clearly reveal the origin for the prominent hysteresis effect in the D_2 isotherm experiments. It is necessary to have a certain amount of pressure to open the structure to the OP-D_2 phase because it is originally closed when the gas loading occurs at 77 K.[50] Once the structure is opened, the interaction between gas molecules and framework is sufficient such that even when the pressure is reduced, the framework does not return to the original CP structure. Therefore, the desorption branch of MIL-53(Al) can retain more D_2 gas under the same pressure after the "pore-opening" process in the adsorption branch at 77 K.

D_2 Pump Evacuation Experiments. While the temperature was maintained at 77 K, a high vacuum (using a turbomolecular pump) was applied to the MIL-53(Al) sample for approximately 30 min. After that, the valve to the pump was closed and NPD data were collected. The diffraction pattern shows significant changes when compared with the 1.5 bar desorption branch data (Figure 1). The Rietveld refinement, presented in Figure 4a (crystallographic data, Tables S17–S20 of the Supporting Information), indicates that a portion of the sample returned to the full OP structure with *Imma* symmetry and does not contain any D_2 gas molecules in the pore, while the remainder has transformed into the CP structure with (at least) three discernibly different lattice parameters which are characterized primarily by large variations in the pore breathing direction, i.e., the *b*-axis. Even when the model has three

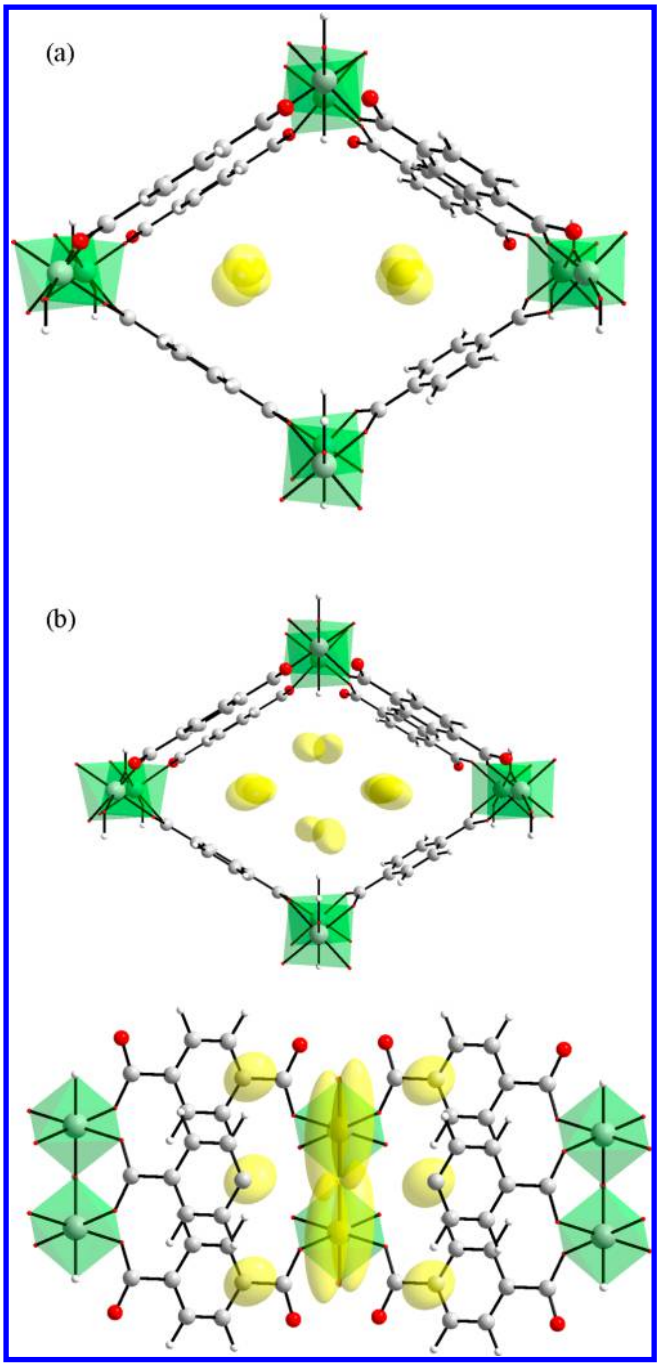

Figure 3. (a) Structure view of D_2 adsorbed MIL-53(Al) along the rhombus channel direction (perpendicular view available in the Supporting Information) at 0.5 bar D_2 pressure measured at 77 K. The AlO_6 octahedra are shaded green; carbon atoms are shown as gray spheres, and framework D atoms as white. Partially transparent yellow sphere represents the first adsorption site for D_2. (b) Structure of D_2 adsorbed MIL-53(Al) view along (top panel) and perpendicular to (bottom panel) the rhombus channel direction at 4.5 bar D_2 pressure measured at 77 K. Partially transparent yellow ellipsoids represent the D_2 molecules, with the second adsorption site defined by the ADP being elongated along the channel axis.

dx.doi.org/10.1021/jp504870n | J. Phys. Chem. C 2014, 118, 18197–18206

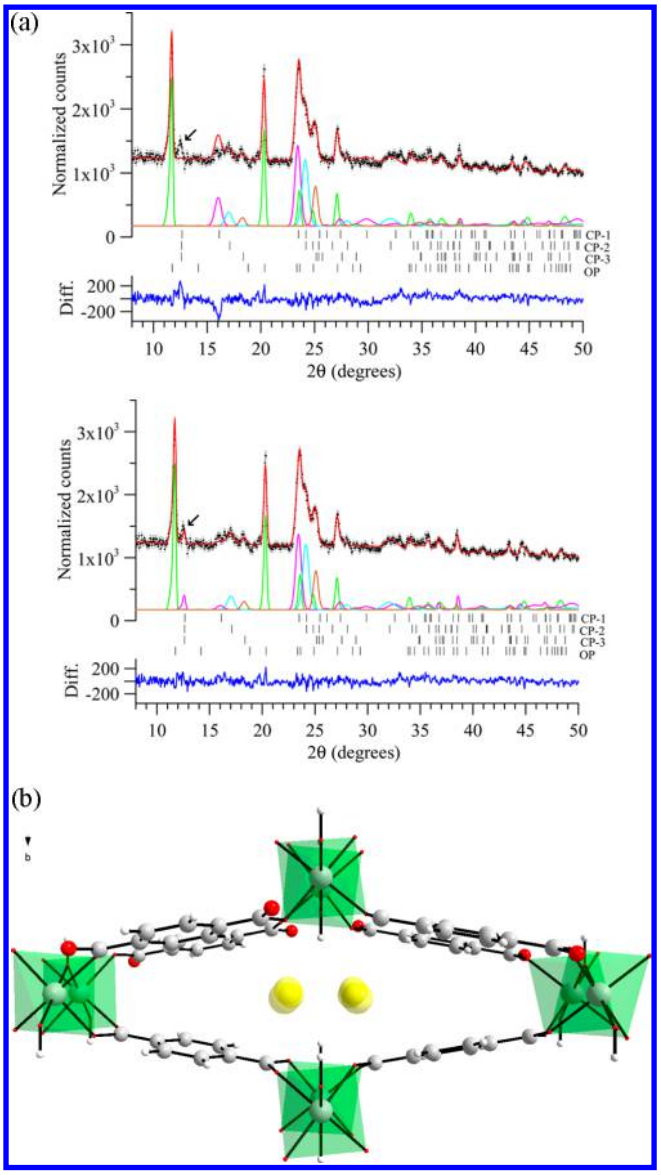

Figure 4. (a) NPD patterns of MIL-53(Al) measured after pumping out the D_2 gas for ~30 min (black circles with error bars indicating one standard deviation) at 77 K. Pink, cyan, and orange curves illustrate the contributions from the three modeled closed pore phases (tickmarks given for CP-1, CP-2, and CP-3), while the green is for the completely open pore (OP tickmarks). The arrow indicates the (200) reflection of CP structure, whose observed intensity cannot be explained by the structural model without residual trapped D_2 molecules (top panel) but is satisfactorily predicated using a model with residual D_2 molecules in the narrow pore (bottom panel). The blue curve is the difference between data and calculated patterns. (b) Structure view along the rhombus channel direction (perpendicular view available in the Supporting Information) of D_2 adsorbed MIL-53 (CP-1) measured after pumping out the D_2 gas at 77 K for 30 min. Partially transparent yellow spheres represent the D_2 molecules.

different lattice parameters for the narrow CP phase, the NPD pattern could not be satisfactorily explained if the pore structure is void of D_2 molecules. Specifically, the Rietveld analysis is unable to reproduce the intensities of the (200) and (110) reflections as shown in Figure 4a (top panel). Because the pristine CP structure model predicts almost no intensity in the (200) reflection, the neutron scattering contribution to that reflection from the Al−O_6 planes and BDC benzene planes are almost equal. Hence, we expect that some unaccounted for scattering density remains in the *narrow* CP structure with a periodicity of one-half of the *a*-axis, which gives additional neutron scattering contrast between the Al−O_6 and BDC benzene layers. This unidentified scattering density is most likely due to remnant D_2 molecules, even though the sample cell was pumped out for about 30 min at 77 K. Using SA, as described previously, we can locate the D_2 molecules in the CP-1 phase. The newly added D_2 molecules explained the observed pattern, as shown in Figure 4a (bottom panel). This is the first direct observation for trapped/clamped D_2 molecules in a MOF system resulting from a structural phase transition. The modeled, trapped D_2 molecules in the CP structure after Rietveld refinement are presented in Figure 4b. A schematic diagram to explain the existence of three different phases of CP MIL-53(Al) is presented in Figure S16 of the Supporting Information in which CP-1 has the largest pore size among the three CP phases.

The above idea can be tested and supported by subsequent experiments at 100 and 120 K. By heating the sample, the trapped D_2 will eventually be liberated as the thermal energy increases and along with the framework phonons and vibrations. After 30 min of pumping at each temperature, NPD patterns were collected. The (200) diffraction peak in the 100 and 120 K data show very weak and no noticeable intensity, respectively (Figure S17 of the Supporting Information), reflecting the gradual removal of the trapped D_2 molecules at 100 K and complete removal by 120 K. The 3-phase contribution of observed CP phases was also reduced upon losing the trapped D_2. Both patterns can be analyzed with one phase for each OP and CP structure (crystallographic data, Tables S21−S24 of the Supporting Information). It is important to note that even though we modeled the D_2 as residing only in the CP-1 phase for the data collected at 77 K, there is likely a distribution of D_2 occupancies in the CP-1, -2, and -3 phases, though a realistic modeling of such a D_2 distribution would be beyond the current data.

QENS H_2 Dynamics. The QENS experiments were similar to the NPD D_2 isotherm measurements in that an increasing pressure of H_2 gas was applied to the MIL-53(Al) sample at 77 K, from 0.0 to 4.74 bar, and then the H_2 was evacuated from the sample following the desorption branch of the isotherm. QENS data were collected periodically throughout the adsorption−desorption process (locations on the H_2 isotherm are shown in Figure S18 of the Supporting Information). The data, at all H_2 pressures and momentum transfers (Q), can be fitted using a delta-function, a broad Lorentzian, and a narrow Lorentzian, all convoluted with the instrument resolution function. The resolution function used in the convolution of the components was taken as the spectra of the bare MIL-53(Al) at 77 K, which essentially exhibited a Gaussian instrumental line-shape and no indications of a QENS component. The Lorentzian peaks represent diffusive H_2 motion on different time scales; the faster the motion, the broader the Lorentzian. As the H_2 pressure increases, the overall scattering intensity increases (Figure 5a) and the broad Lorentzian dominates the overall intensity. This is a bulklike molecular diffusion process occurring on a time scale faster than that of the mobile surface hydrogen, which is described by the narrow Lorentzian. The intensity of the broad H_2 rises in proportion to the pressure in the sample cell and is likely due to free-H_2 in the cell.

dx.doi.org/10.1021/jp504870n | J. Phys. Chem. C 2014, 118, 18197−18206

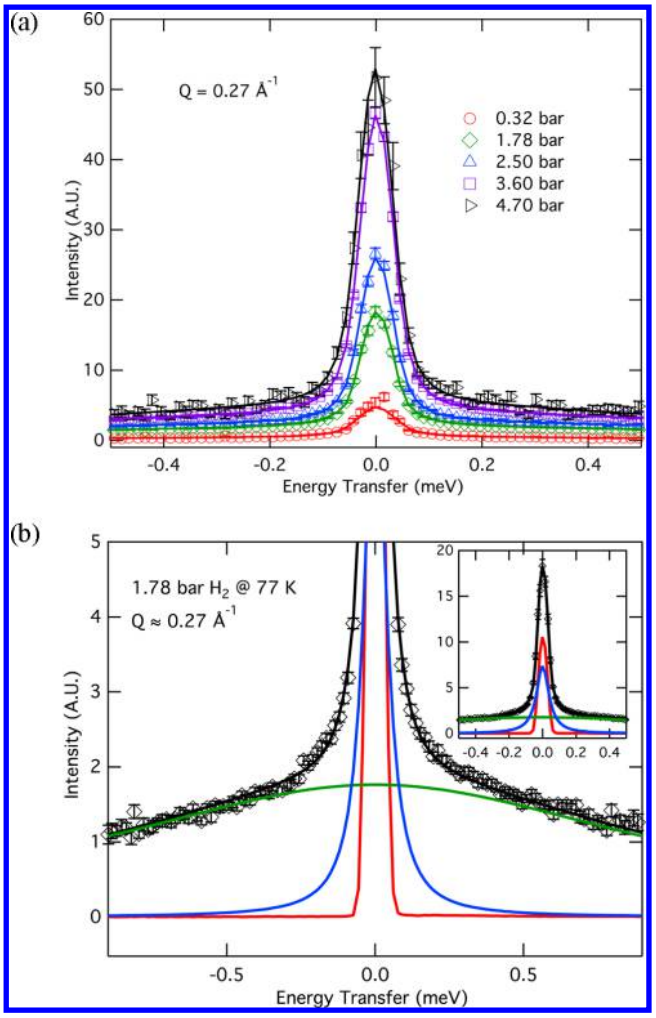

Figure 5. (a) QENS data for H_2 adsorbed at 77 K in MIL-53(Al) for various pressures and a momentum transfer of 0.27 Å^{-1}. The solid lines are the total fit for the spectra using the fitting model described in the text (further details in the Supporting Information). Error bars are shown as vertical lines at the data points for one standard deviation. All Bragg reflections are removed from the data prior to summing in Q. (b) Decomposition of the fit function of the QENS data (black diamonds) for 1.78 bar H_2 at 77 K and Q = 0.27 Å^{-1}. The total fit is shown with a black solid line, the resolution function is in red, broad Lorentzian in green, and the narrow Lorentzian for the adsorbed H_2 in blue. Error bars are shown as vertical lines at the data points for one standard deviation. Inset shows the full intensity scale for the same data.

The data and fits (delta and two Lorentzians) for a H_2 pressure of 1.78 bar at 77 K and a momentum transfer of 0.27 Å^{-1} are given in Figure 5b, where the total fit reproduces both the intensity of the elastic peak and the shape of the broadening. There is an almost linear decrease in the elastic intensity as Q increases, while the intensity of the narrow Lorentzian remains relatively constant at small Q and then decreases linearly.

Information about the dynamics of the H_2 in the system is obtained from the width of the Lorentzian versus Q^2. The widths of the narrow component generally increase at low Q and then reach an asymptote at larger Q (Figure 6). This behavior is characteristic of a jump-diffusion with no distinct spatial orientation of the jump directions as reported in other studies of H_2 in porous media.[84,85] The half-width at half-

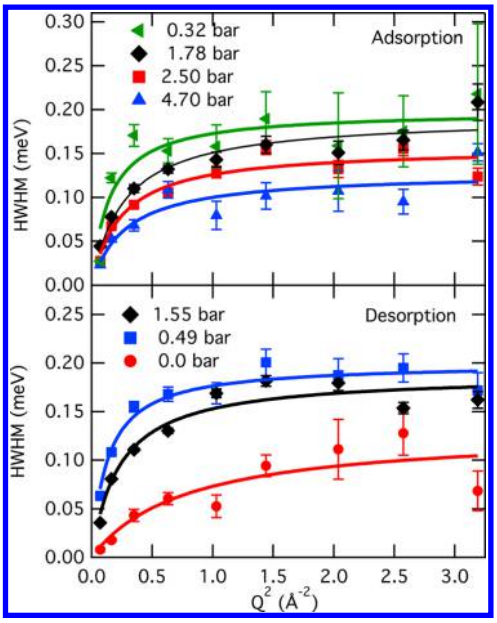

Figure 6. Half-width at half-maximum of the narrow Lorentzian for fits to the QENS data of both the adsorption branch (top panel) and desorption branch (bottom panel) of the H_2 isotherms versus Q^2. Solid lines are fits to the data using a liquidlike jump-diffusion model as described in the text. Error bars indicate one standard deviation of the values from a least-squares fitting of the data to the phenomenological fit function.

maximum (HWHM) of the Lorentzian broadening as a function of Q is given in eq 1

$$\mathrm{HWHM}(Q) = \frac{\hbar}{\tau_o}\left(1 - \frac{1}{1 + Q^2 l_o^2}\right) \quad (1)$$

where τ_o is the residency time at a given site and the jump length, l, has a distribution of values given by $l\exp(l/l_o)$,where l_o is the characteristic jump length.[85,86] The effective self-diffusivity (D_{eff}) is calculated from the characteristic jump length and the residency time and is expressed as $D_{\mathrm{eff}} = l_o^2/\tau_o$. The HWHM data were fit to this model, and the characteristic jump lengths, residency times, and effective self-diffusion coefficients for H_2 pressures during both adsorption and desorption are given in Table 1. As the H_2 pressure increases from 0.32 to 4.74 bar, the residency time also increases from about 3 to 5 ps, while the jump length decreases from ca. 2.6 to

Table 1. Characteristic Lengths, Residency Times, and Effective Diffusivity Values for the Given Pressures, along the Hydrogen Sorption Isotherm Calculated from the HWHM of the Narrow Lorentzian Used to Fit the QENS Data[a]

H_2 pressure (bar)	l_o (Å)	τ_o (ps)	D_{eff} ($\times 10^{-8}$ m^2/s)
ads-0.32	2.6(5)	3.3(3)	2.0(9)
ads-1.78	1.9(2)	3.4(2)	1.1(3)
ads-2.5	2.0(3)	4.2(3)	1.0(3)
ads-4.74	1.9(5)	5.1(6)	0.7(3)
des-1.55	2.1(3)	3.5(2)	1.2(3)
des-0.49	2.8(3)	3.3(1)	2.3(4)
des-0.0	1.1(4)	5(1)	0.3(2)

[a]The numbers in parentheses indicate one standard deviation from the least-squares fitting of the data to the phenomenological fit function.

dx.doi.org/10.1021/jp504870n | J. Phys. Chem. C 2014, 118, 18197−18206

1.9 Å. This is consistent with a picture of the liquidlike three-dimensional (3D) jump diffusion of hydrogen in the pores with the motion becoming restricted as more H_2 is added to the unit cell and causing a concomitant decrease in diffusivity from $2.0(8) \times 10^{-8}$ m^2/s to $0.7(3) \times 10^{-8}$ m^2/s. When decreasing pressure, along the desorption branch of the isotherm, these values begin to return to their original values; however, when the hydrogen pressure is zero, there is a significant decrease in l_o and a dramatic increase in τ_o. When MIL-53(Al) is evacuated at 77 K, it undergoes a change from the OP-D_2 to the CP structure and some residual hydrogen remains in the system. The smaller pore volume restricts the motion of the H_2 molecules, which explains the almost order of magnitude decrease in the effective diffusivity from its most mobile at 2.0×10^{-8} m^2/s to the most restricted measured at 3×10^{-9} m^2/s when the H_2 pressure is decreased to 0.0 bar.

The effective diffusivity calculated here for H_2 in MIL-53(Al) at 77 K, $2.0(9) \times 10^{-8}$ m^2/s at 0.32 bar H_2, is slightly faster than H_2 at the same temperature in porous carbon (7.7×10^{-9} m^2/s at 0.5 wt % H_2),[85] but these results are similar to self-diffusivities reported in the literature for H_2 in MIL-53(Cr).[72,73] However, it is important to note in the latter example that instead of using a 3D jump diffusion model, Salles et al. employed a one-dimensional model of diffusion as described by Jobic.[87] When the system is in the OP-D_2 phase, observed at higher loadings, there are multiple adsorption sites, and we conclude that the H_2 is able to diffuse in the OP-D_2 framework in all three dimensions, justifying the Lorentzian phenomenological fitting function. The dynamics change when the hydrogen is evacuated from the framework and residual gas is trapped in the narrow CP phase. When H_2 is trapped in the framework, we might expect that the diffusion would be one-dimensional; however, the 3D models employed here do reproduce the scattered intensity quite accurately (Figure S19 of the Supporting Information) over the Q-range covered. The instrument resolution in the MIL-53(Cr) experiments (ca. 45 μeV)[73] is significantly better than that used for these experiments (ca. 70 μeV), and the MIL-53(Cr) data were also analyzed at a much smaller Q range (longer length-scale). It may be possible that with a better instrument resolution, and better statistics at the lowest Q, a 1D diffusion process in this MIL-53(Al) system could be observable.

N_2 Pressure Experiments. NPD measurements along the N_2 isotherm suggest extremely strong gas−framework interactions, in contrast to similar experiments with D_2. The N_2 gas was loaded at 80 K, slightly above its condensation temperature, and NPD data of MIL-53(Al) were measured under vacuum and 0.2 and 0.5 bar N_2 (Figure S20 of the Supporting Information). As there is significant disorder of the N_2 molecule, using a similar super atom approach as for the D_2 analysis, we can still capture the essential features of the adsorption with a large thermal parameter (Rietveld refinement and structure, Figures S21 and S22, respectively, and crystallographic data, Table S25 of the Supporting Information). The Fourier difference map is presented in Figure 7 for the lowest loading of N_2 in MIL-53(Al). As low as 0.2 bar, it is evident that the N_2 molecule caused the framework to open completely, implying that the N_2−framework interaction is much stronger than the energy required for the conversion of the open ↔ closed pore structure.

The adsorption scheme is similar to that of D_2 in MIL-53(Al), on top of benzene ring of BDC and around Al−O_6 cluster with elongated distribution along the channel direction,

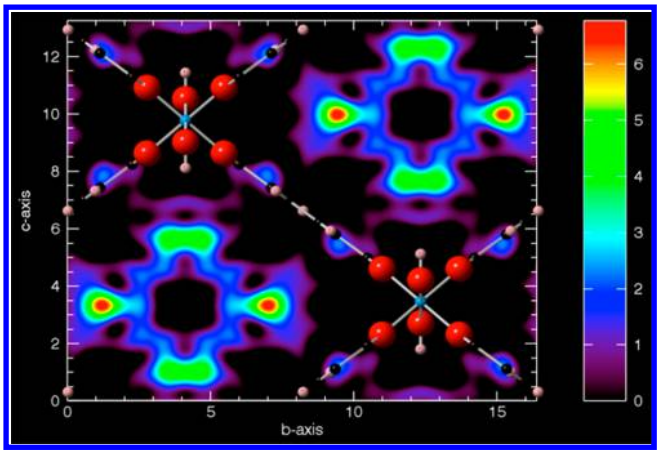

Figure 7. Fourier difference map of 0.2 bar N_2 in MIL-53(Al) measured at 80 K. Colors represent neutron densities of N_2 imaged down the length of the pore with the atomic structure of MIL-53(Al) superimposed for positional clarity.

but the open structure has a fully open *Imma* symmetry, not the partially closed *C*2/*c* symmetry as observed for the D_2 loaded MIL-53(Al). The benzene rings are completely parallel to the *c*-axis, not canted as observed in the D_2 adsorption experiments. We speculate that this binding scheme is common when primarily nonpolar molecules are loaded into MIL-53(Al) while polar (or charge-separated) molecules (e.g., CO_2, H_2O) clearly show a different adsorption state, i.e., in the middle of CP structure, that maximizes the electrostatic interactions between guest molecules and framework, causing pore closing.

He Pressure Experiments. NPD data under He pressure, Figure 8, were collected from 0 to 10 bar at 77 K. In contrast to

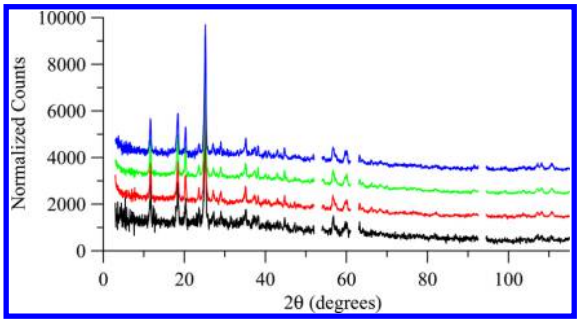

Figure 8. NPD patterns of MIL-53(Al) measured at 77 K under vacuum (black), 0.5 bar (red), 4.5 bar (green), and 10 bar (blue) He pressure. (Gaps in the pattern correspond to the aluminum Bragg reflections from the sample container.).

D_2 or N_2 experiments, the NPD pattern does not change with increasing He pressure. The unchanging powder pattern indicates that He gas does not interact with MIL-53(Al) at 77 K and up to 10 bar pressure. This suggests that the interaction strength between the nonpolar gas molecules and MIL-53(Al) followed the order of condensation temperature of each gas type when compared in the temperature range of interest for isotherm measurements, around 77 K. The N_2 gas, with the highest boiling point (77 K), interacts most strongly with MIL-53(Al) among the tested gases, and He gas, with the lowest boiling point (4 K), does not interact with the framework. D_2, having an intermediate boiling point (20 K), shows moderate interactions that cause the interesting pressure-dependent structural responses of MIL-53(Al).

dx.doi.org/10.1021/jp504870n | J. Phys. Chem. C 2014, 118, 18197−18206

CONCLUSION

Because MIL-53(Al) is a crystalline, breathing (flexible) MOF, it is an ideal system to study the structural response as a function of gas-loading environment with diffraction and QENS techniques. This is not only interesting for potential gas storage purposes but also important for understanding the fundamental physics of this type of novel breathing phenomena and interaction between framework and guest molecules. The in situ gas loading NPD experiments, analyzed using the Rietveld method and quantitatively modeled, revealed the binding sites of D_2 and N_2 gas in MIL-53(Al) and the structural origins of hysteresis in the isotherm. We have shown that nonpolar and polar (charge-separated) guest molecules adsorb in different ways and that the framework interacts with guest molecules with different strength resulting in rich structural behaviors. One of the more interesting observations is that there is residual D_2 clamped by the framework that was directly observed experimentally for the first time. QENS data showed that the mobility of the hydrogen in this clamped mode is less than that when the molecule is in the open structure. This suggests that kinetic trapping of H_2 may be possible with flexible MOFs employing a structural phase transition, though the amounts trapped may be small.

ASSOCIATED CONTENT

Supporting Information

Details of Rietveld analysis and crystallographic data. This material is available free of charge via the Internet at http://pubs.acs.org.

AUTHOR INFORMATION

Corresponding Author

*Tel: +1 (301) 975-5134. E-mail: craig.brown@nist.gov.

Present Address

[⊥]J.-H.H.: GE Global Research, Niskayuna, NY 12309 USA

Notes

The authors declare no competing financial interest.

ACKNOWLEDGMENTS

This work was partially supported by the U.S. Department of Energy, Office of Energy Efficiency and Renewable Energy within the Hydrogen Sorption Center of Excellence. This work utilized facilities supported in part by the National Science Foundation under Agreement DMR-0944772. We thank M.R. Hudson for comments concerning this manuscript.

REFERENCES

(1) Barthelet, K.; Marrot, J.; Riou, D.; Ferey, G. A Breathing Hybrid Organic-Inorganic Solid with Very Large Pores and High Magnetic Characteristics. *Angew. Chem., Int. Ed.* **2002**, *41*, 281−284.

(2) Eddaoudi, M.; Moler, D. B.; Li, H. L.; Chen, B. L.; Reineke, T. M.; O'Keeffe, M.; Yaghi, O. M. Modular Chemistry: Secondary Building Units as a Basis for the Design of Highly Porous and Robust Metal-Organic Carboxylate Frameworks. *Acc. Chem. Res.* **2001**, *34*, 319−330.

(3) Ferey, G. Hybrid Porous Solids: Past, Present, Future. *Chem. Soc. Rev.* **2008**, *37*, 191−214.

(4) Hoskins, B. F.; Robson, R. J. Infinite Polymeric Frameworks Consisting of 3 Dimensionally Linked Rod-Like Segments. *J. Am. Chem. Soc.* **1989**, *111*, 5962−5964.

(5) Kepert, C. J.; Rosseinsky, M. J. Zeolite-Like Crystal Structure of an Empty Microporous Molecular Framework. *Chem. Commun. (Cambridge, U.K.)* **1999**, 375−376.

(6) Kitagawa, S.; Kitaura, R.; Noro, S. Functional Porous Coordination Polymers. *Angew. Chem., Int. Ed.* **2004**, *43*, 2334−2375.

(7) Yaghi, O. M.; Li, G. M.; Li, H. L. Selective Binding and Removal of Guests in a Microporous Metal-Organic Framework. *Nature (London, U.K.)* **1995**, *378*, 703−706.

(8) Dinca, M.; Dailly, A.; Liu, Y.; Brown, C. M.; Neumann, D. A.; Long, J. R. Hydrogen Storage in a Microporous Metal−Organic Framework with Exposed Mn^{2+} Coordination Sites. *J. Am. Chem. Soc.* **2006**, *128*, 16876−16883.

(9) Murray, L. J.; Dinca, M.; Long, J. R. Hydrogen Storage in Metal-Organic Frameworks. *Chem. Soc. Rev.* **2009**, *38*, 1294−1314.

(10) Rosi, N. L.; Eckert, J.; Eddaoudi, M.; Vodak, D. T.; Kim, J.; O'Keeffe, M.; Yaghi, O. M. Hydrogen Storage in Microporous Metal-Organic Frameworks. *Science* **2003**, *300*, 1127−1129.

(11) Sumida, K.; Her, J. H.; Dinca, M.; Murray, L. J.; Schloss, J. M.; Pierce, C. J.; Thompson, B. A.; FitzGerald, S. A.; Brown, C. M.; Long, J. R. Neutron Scattering and Spectroscopic Studies of Hydrogen Adsorption in $Cr_3(BTC)_2$—A Metal−Organic Framework with Exposed Cr^{2+} Sites. *J. Phys. Chem. C* **2011**, *115*, 8414−8421.

(12) Queen, W. L.; Bloch, E. D.; Brown, C. M.; Hudson, M. R.; Mason, J. A.; Murray, L. J.; Ramirez-Cuesta, A. J.; Peterson, V. K.; Long, J. R. Hydrogen Adsorption in the Metal-Organic Frameworks Fe_2(dobdc) and $Fe_2(O_2)$(dobdc). *Dalton Trans.* **2012**, *41*, 4180−4187.

(13) Brown, C. M.; Ramirez-Cuesta, A. J.; Her, J. H.; Wheatley, P. S.; Morris, R. E. Structure and Spectroscopy of Hydrogen Adsorbed in a Nickel Metal-Organic Framework. *Chem. Phys.* **2013**, *427*, 3−8.

(14) Eddaoudi, M.; Kim, J.; Rosi, N.; Vodak, D.; Wachter, J.; O'Keeffe, M.; Yaghi, O. M. Systematic Design of Pore Size and Functionality in Isoreticular MOFs and Their Application in Methane Storage. *Science* **2002**, *295*, 469−472.

(15) Ma, S. Q.; Sun, D. F.; Simmons, J. M.; Collier, C. D.; Yuan, D. Q.; Zhou, H. C. Metal-Organic Framework From an Anthracene Derivative Containing Nanoscopic Cages Exhibiting High Methane Uptake. *J. Am. Chem. Soc.* **2008**, *130*, 1012−1016.

(16) Wu, H.; Simmons, J. M.; Liu, Y.; Brown, C. M.; Wang, X. S.; Ma, S.; Peterson, V. K.; Southon, P. D.; Kepert, C. J.; Zhou, H. C.; et al. Metal-Organic Frameworks with Exceptionally High Methane Uptake: Where and How is Methane Stored? *Chem.—Eur. J.* **2010**, *16*, 5205−5214.

(17) Wu, H.; Zhou, W.; Yildirim, T. High-Capacity Methane Storage in Metal−Organic Frameworks M_2(dhtp): The Important Role of Open Metal Sites. *J. Am. Chem. Soc.* **2009**, *131*, 4995−5000.

(18) D'Alessandro, D. M.; Smit, B.; Long, J. R. Carbon Dioxide Capture: Prospects for New Materials. *Angew. Chem., Int. Ed.* **2010**, *49*, 6058−6082.

(19) Millward, A. R.; Yaghi, O. M. Metal−Organic Frameworks with Exceptionally High Capacity for Storage of Carbon Dioxide at Room Temperature. *J. Am. Chem. Soc.* **2005**, *127*, 17998−17999.

(20) Wang, B.; Cote, A. P.; Furukawa, H.; O'Keeffe, M.; Yaghi, O. M. Colossal Cages in Zeolitic Imidazolate Frameworks as Selective Carbon Dioxide Reservoirs. *Nature (London, U.K.)* **2008**, *453*, 207−211.

(21) Caskey, S. R.; Wong-Foy, A. G.; Matzger, A. J. Dramatic Tuning of Carbon Dioxide Uptake Via Metal Substitution in a Coordination Polymer with Cylindrical Pores. *J. Am. Chem. Soc.* **2008**, *130*, 10870−10871.

(22) Bae, Y. S.; Lee, C. Y.; Kim, K. C.; Farha, O. K.; Nickias, P.; Hupp, J. T.; Nguyen, S. T.; Snurr, R. Q. High Propene/Propane Selectivity in Isostructural Metal-Organic Frameworks with High Densities of Open Metal Sites. *Angew. Chem., Int. Ed.* **2012**, *51*, 1857−1860.

(23) Bloch, E. D.; Queen, W. L.; Krishna, R.; Zadrozny, J. M.; Brown, C. M.; Long, J. R. Hydrocarbon Separations in a Metal-Organic Framework with Open Iron(II) Coordination Sites. *Science* **2012**, *335*, 1606−1610.

(24) Dietzel, P. D. C.; Besikiotis, V.; Blom, R. Application of Metal-Organic Frameworks with Coordinatively Unsaturated Metal Sites in Storage and Separation of Methane and Carbon Dioxide. *J. Mater. Chem.* **2009**, *19*, 7362−7370.

(25) He, Y. B.; Zhang, Z. J.; Xiang, S. C.; Fronczek, F. R.; Krishna, R.; Chen, B. L. A Microporous Metal-Organic Framework for Highly Selective Separation of Acetylene, Ethylene, and Ethane from Methane at Room Temperature. *Chem.—Eur. J.* **2012**, *18*, 613−619.
(26) Nuzhdin, A. L.; Kovalenko, K. A.; Dybtsev, D. N.; Bukhtiyarova, G. A. Removal of Nitrogen Compounds from Liquid Hydrocarbon Streams by Selective Sorption on Metal-Organic Framework MIL-101. *Mendeleev Commun.* **2010**, *20*, 57−58.
(27) Bloch, E. D.; Murray, L. J.; Queen, W. L.; Chavan, S.; Maximoff, S. N.; Bigi, J. P.; Krishna, R.; Peterson, V. K.; Grandjean, F.; Long, G. J.; et al. Selective Binding of O_2 over N_2 in a Redox−Active Metal−Organic Framework with Open Iron(II) Coordination Sites. *J. Am. Chem. Soc.* **2011**, *133*, 14814−14822.
(28) Marcz, M.; Johnsen, R. E.; Dietzel, P. D. C.; Fjellvag, H. The Iron Member of the CPO-27 Coordination Polymer Series: Synthesis, Characterization, and Intriguing Redox Properties. *Microporous Mesoporous Mater.* **2012**, *157*, 62−74.
(29) Salles, F.; Jobic, H.; Devic, T.; Guillerm, V.; Serre, C.; Koza, M. M.; Ferey, G.; Maurin, G. Diffusion of Binary CO_2/CH_4 Mixtures in the MIL-47(V) and MIL-53(Cr) Metal−Organic Framework Type Solids: A Combination of Neutron Scattering Measurements and Molecular Dynamics Simulations. *J. Phys. Chem. C* **2013**, *117*, 11275−11284.
(30) Hulvey, Z.; Lawler, K. V.; Qao, Z. W.; Zhou, J.; Fairen-Jimenez, D.; Snurr, R. Q.; Ushakov, S. V.; Navrotsky, A.; Brown, C. M.; Forster, P. M. Noble Gas Adsorption in Copper Trimesate, HKUST-1: An Experimental and Computational Study. *J. Phys. Chem. C* **2013**, *117*, 20116−20126.
(31) Geier, S. J.; Mason, J. A.; Bloch, E. D.; Queen, W. L.; Hudson, M. R.; Brown, C. M.; Long, J. R. Selective Adsorption of Ethylene over Ethane and Propylene over Propane in the Metal-Organic Frameworks M_2(dobdc) (M = Mg, Mn, Fe, Co, Ni, Zn). *Chem. Sci.* **2013**, *4*, 2054−2061.
(32) Chen, B. L.; Yang, Y.; Zapata, F.; Lin, G. N.; Qian, G. D.; Lobkovsky, E. B. Luminescent Open Metal Sites within A Metal-Organic Framework For Sensing Small Molecules. *Adv. Mater. (Weinheim, Ger.)* **2007**, *19*, 1693−1696.
(33) Maspoch, D.; Ruiz-Molina, D.; Wurst, K.; Domingo, N.; Cavallini, M.; Biscarini, F.; Tejada, J.; Rovira, C.; Veciana, J. A Nanoporous Molecular Magnet with Reversible Solvent-Induced Mechanical and Magnetic Properties. *Nat. Mater.* **2003**, *2*, 190−195.
(34) Horcajada, P.; Gref, R.; Baati, T.; Allan, P. K.; Maurin, G.; Couvreur, P.; Ferey, G.; Morris, R. E.; Serre, C. Metal−Organic Frameworks in Biomedicine. *Chem. Rev. (Washington, DC, U.S.)* **2012**, *112*, 1232−1268.
(35) Fujita, M.; Kwon, Y. J.; Washizu, S.; Ogura, K. Preparation, Clathration Ability, and Catalysis of A 2-Dimensional Square Network Material Composed of Cadmium(ii) and 4,4′-Bipyridine. *J. Am. Chem. Soc.* **1994**, *116*, 1151−1152.
(36) Seo, J. S.; Whang, D.; Lee, H.; Jun, S. I.; Oh, J.; Jeon, Y. J.; Kim, K. A Homochiral Metal-Organic Porous Material for Enantioselective Separation and Catalysis. *Nature (London, U.K.)* **2000**, *404*, 982−986.
(37) Wu, C. D.; Hu, A.; Zhang, L.; Lin, W. B. Homochiral Porous Metal−Organic Framework for Highly Enantioselective Heterogeneous Asymmetric Catalysis. *J. Am. Chem. Soc.* **2005**, *127*, 8940−8941.
(38) Serre, C.; Millange, F.; Thouvenot, C.; Nogues, M.; Marsolier, G.; Louer, D.; Ferey, G. Very Large Breathing Effect in the First Nanoporous Chromium(III)-Based Solids: MIL-53 or $Cr^{III}(OH)\cdot\{O_2C-C_6H_4-CO_2\}\cdot\{HO_2C-C_6H_4-CO_2H\}_x\cdot H_2O_y$. *J. Am. Chem. Soc.* **2002**, *124*, 13519−13526.
(39) Demessence, A.; Long, J. R. Selective Gas Adsorption in the Flexible Metal-Organic Frameworks Cu(BDTri)L (L = DMF, DEF). *Chem.—Eur. J.* **2010**, *16*, 5902−5908.
(40) Fletcher, A. J.; Thomas, K. M.; Rosseinsky, M. J. Flexibility in Metal-Organic Framework Materials: Impact on Sorption Properties. *J. Solid State Chem.* **2005**, *178*, 2491−2510.
(41) Kauffman, K. L.; Culp, J. T.; Allen, A. J.; Espinal, L.; Wong-Ng, W.; Brown, T. D.; Goodman, A.; Bernardo, M. P.; Pancoast, R. J.; Chirdon, D.; et al. Selective Adsorption of CO_2 from Light Gas Mixtures by Using a Structurally Dynamic Porous Coordination Polymer. *Angew. Chem., Int. Ed.* **2011**, *50*, 10888−10892.
(42) Klein, N.; Hoffmann, H. C.; Cadiau, A.; Getzschmann, J.; Lohe, M. R.; Paasch, S.; Heydenreich, T.; Adil, K.; Senkovska, I.; Brunner, E.; et al. Structural Flexibility and Intrinsic Dynamics in the M_2(2,6-ndc)$_2$(dabco) (M = Ni, Cu, Co, Zn) Metal−Organic Frameworks. *J. Mater. Chem.* **2012**, *22*, 10303−10312.
(43) Mellot-Draznieks, C.; Serre, C.; Surble, S.; Audebrand, N.; Ferey, G. Very Large Swelling in Hybrid Frameworks: A Combined Computational and Powder Diffraction Study. *J. Am. Chem. Soc.* **2005**, *127*, 16273−16278.
(44) Seo, J.; Matsuda, R.; Sakamoto, H.; Bonneau, C.; Kitagawa, S. A Pillared-Layer Coordination Polymer with a Rotatable Pillar Acting as a Molecular Gate for Guest Molecules. *J. Am. Chem. Soc.* **2009**, *131*, 12792−12800.
(45) Serre, C.; Mellot-Draznieks, C.; Surble, S.; Audebrand, N.; Filinchuk, Y.; Ferey, G. Role of Solvent-Host Interactions That Lead to Very Large Swelling of Hybrid Frameworks. *Science* **2007**, *315*, 1828−1831.
(46) Zhao, X. B.; Xiao, B.; Fletcher, A. J.; Thomas, K. M.; Bradshaw, D.; Rosseinsky, M. J. Hysteretic Adsorption and Desorption of Hydrogen by Nanoporous Metal-Organic Frameworks. *Science* **2004**, *306*, 1012−1015.
(47) Choi, H. J.; Dinca, M.; Long, J. R. Broadly Hysteretic H_2 Adsorption in the Microporous Metal−Organic Framework Co(1,4-benzenedipyrazolate). *J. Am. Chem. Soc.* **2008**, *130*, 7848−7850.
(48) Bon, V.; Senkovska, I.; Wallacher, D.; Többens, D. M.; Zizak, I.; Feyerherm, R.; Mueller, U.; Kaskel, S. In Situ Observation of Gating Phenomena in the Flexible Porous Coordination Polymer Zn_2(BPnDC)$_2$(bpy) (SNU-9) in a Combined Diffraction and Gas Adsorption Experiment. *Inorg. Chem.* **2014**, *53*, 1513−1520.
(49) Ghoufi, A.; Subercaze, A.; Ma, Q.; Yot, P. G.; Ke, Y.; Puente-Orench, I.; Devic, T.; Guillerm, V.; Zhong, C.; Serre, C.; et al. Comparative Guest, Thermal, and Mechanical Breathing of the Porous Metal Organic Framework MIL-53(Cr): A Computational Exploration Supported by Experiments. *J. Phys. Chem. C* **2012**, *116*, 13289−13295.
(50) Liu, Y.; Her, J. H.; Dailly, A.; Ramirez-Cuesta, A. J.; Neumann, D. A.; Brown, C. M. Reversible Structural Transition in MIL-53 with Large Temperature Hysteresis. *J. Am. Chem. Soc.* **2008**, *130*, 11813−11818.
(51) Mishra, P.; Edubilli, S.; Uppara, H. P.; Mandal, B.; Gumma, S. Effect of Adsorbent History on Adsorption Characteristics of MIL-53(Al) Metal Organic Framework. *Langmuir* **2013**, *29*, 12162−12167.
(52) Bourrelly, S.; Llewellyn, P. L.; Serre, C.; Millange, F.; Loiseau, T.; Ferey, G. Different Adsorption Behaviors of Methane and Carbon Dioxide in the Isotypic Nanoporous Metal Terephthalates MIL-53 and MIL-47. *J. Am. Chem. Soc.* **2005**, *127*, 13519−13521.
(53) Loiseau, T.; Serre, C.; Huguenard, C.; Fink, G.; Taulelle, F.; Henry, M.; Bataille, T.; Ferey, G. A Rationale for the Large Breathing of the Porous Aluminum Terephthalate (MIL-53) upon Hydration. *Chem.—Eur. J.* **2004**, *10*, 1373−1382.
(54) Springuel-Huet, M. A.; Nossov, A.; Adem, Z.; Guenneau, F.; Volkringer, C.; Loiseau, T.; Ferey, G.; Gedeon, A. ^{129}Xe NMR Study of the Framework Flexibility of the Porous Hybrid MIL-53(Al). *J. Am. Chem. Soc.* **2010**, *132*, 11599−11607.
(55) Llewellyn, P. L.; Bourrelly, S.; Serre, C.; Filinchuk, Y.; Ferey, G. How Hydration Drastically Improves Adsorption Selectivity for CO_2 over CH_4 in the Flexible Chromium Terephthalate MIL-53. *Angew. Chem., Int. Ed.* **2006**, *45*, 7751−7754.
(56) Couck, S.; Denayer, J. F. M.; Baron, G. V.; Remy, T.; Gascon, J.; Kapteijn, F. An Amine-Functionalized MIL-53 Metal−Organic Framework with Large Separation Power for CO_2 and CH_4. *J. Am. Chem. Soc.* **2009**, *131*, 6326−6327.
(57) Devic, T.; Horcajada, P.; Serre, C.; Salles, F.; Maurin, G.; Moulin, B.; Heurtaux, D.; Clet, G.; Vimont, A.; Greneche, J. M.; et al. Functionalization in Flexible Porous Solids: Effects on the Pore Opening and the Host−Guest Interactions. *J. Am. Chem. Soc.* **2010**, *132*, 1127−1136.

(58) Millange, F.; Serre, C.; Ferey, G. Synthesis, Structure Determination and Properties of MIL-53as and MIL-53ht: The First Cr^{III} Hybrid Inorganic−Organic Microporous Solids: $Cr^{III}(OH)\cdot\{O_2C-C_6H_4-CO_2\}\cdot\{HO_2C-C_6H_4-CO_2H\}_x$. *Chem. Commun. (Cambridge, U.K.)* **2002**, 822−823.
(59) Whitfield, T. R.; Wang, X. Q.; Liu, L. M.; Jacobson, A. J. Metal-Organic Frameworks Based on Iron Oxide Octahedral Chains Connected by Benzenedicarboxylate Dianions. *Solid State Sci.* **2005**, *7*, 1096−1103.
(60) Nouar, F.; Devic, T.; Chevreau, H.; Guillou, N.; Gibson, E.; Clet, G.; Daturi, M.; Vimont, A.; Greneche, J. M.; Breeze, M. I.; et al. Tuning the Breathing Behaviour of MIL-53 by Cation Mixing. *Chem. Commun. (Cambridge, U.K.)* **2012**, *48*, 10237−10239.
(61) Ramsahye, N. A.; Maurin, G.; Bourrelly, S.; Llewellyn, P. L.; Devic, T.; Serre, C.; Loiseau, T.; Ferey, G. Adsorption of CO_2 in Metal Organic Frameworks of Different Metal Centres: Grand Canonical Monte Carlo Simulations Compared to Experiments. *Adsorption* **2007**, *13*, 461−467.
(62) Ramsahye, N. A.; Maurin, G.; Bourrelly, S.; Llewellyn, P. L.; Serre, C.; Loiseau, T.; Devic, T.; Ferey, G. Probing the Adsorption Sites for CO_2 in Metal Organic Frameworks Materials MIL-53(Al, Cr) and MIL-47(V) by Density Functional Theory. *J. Phys. Chem. C* **2008**, *112*, 514−520.
(63) Salles, F.; Jobic, H.; Ghoufi, A.; Llewellyn, P. L.; Serre, C.; Bourrelly, S.; Ferey, G.; Maurin, G. Transport Diffusivity of CO_2 in the Highly Flexible Metal-Organic Framework MIL-53(Cr). *Angew. Chem., Int. Ed.* **2009**, *48*, 8335−8339.
(64) Ghysels, A.; Vanduyfhuys, L.; Vandichel, M.; Waroquier, M.; Van, S. V.; Smit, B. On the Thermodynamics of Framework Breathing: A Free Energy Model for Gas Adsorption in MIL-53. *J. Phys. Chem. C* **2013**, *117*, 11540−11554.
(65) Chen, L.; Mowat, J. P. S.; Fairen-Jimenez, D.; Morrison, C. A.; Thompson, S. P.; Wright, P. A.; Dueren, T. Elucidating the Breathing of the Metal−Organic Framework MIL-53(Sc) with Ab Initio Molecular Dynamics Simulations and in Situ X-ray Powder Diffraction Experiments. *J. Am. Chem. Soc.* **2013**, *135*, 15763−15773.
(66) Coudert, F. X.; Mellot-Draznieks, C.; Fuchs, A. H.; Boutin, A. Double Structural Transition in Hybrid Material MIL-53 upon Hydrocarbon Adsorption: The Thermodynamics Behind the Scenes. *J. Am. Chem. Soc.* **2009**, *131*, 3442−3443.
(67) Llewellyn, P. L.; Maurin, G.; Devic, T.; Loera-Serna, S.; Rosenbach, N.; Serre, C.; Bourrelly, S.; Horcajada, P.; Filinchuk, Y.; Ferey, G. Prediction of the Conditions for Breathing of Metal Organic Framework Materials using a Combination of X-ray Powder Diffraction, Microcalorimetry, and Molecular Simulation. *J. Am. Chem. Soc.* **2008**, *130*, 12808−12814.
(68) Rosenbach, N.; Ghoufi, A.; Deroche, I.; Llewellyn, P. L.; Devic, T.; Bourrelly, S.; Serre, C.; Ferey, G.; Maurin, G. Adsorption of Light Hydrocarbons in the Flexible MIL-53(Cr) and Rigid MIL-47(V) Metal-Organic Frameworks: A Combination of Molecular Simulations and Microcalorimetry/Gravimetry Measurements. *Phys. Chem. Chem. Phys.* **2010**, *12*, 6428−6437.
(69) Trung, T. K.; Trens, P.; Tanchoux, N.; Bourrelly, S.; Llewellyn, P. L.; Loera-Serna, S.; Serre, C.; Loiseau, T.; Fajula, F.; Ferey, G. Hydrocarbon Adsorption in the Flexible Metal Organic Frameworks MIL-53(Al, Cr). *J. Am. Chem. Soc.* **2008**, *130*, 16926−16932.
(70) Ferey, G.; Latroche, M.; Serre, C.; Millange, F.; Loiseau, T.; Percheron-Guegan, A. Hydrogen Adsorption in the Nanoporous Metal-Benzenedicarboxylate $M(OH)(O_2C-C_6H_4-CO_2)$ ($M = Al^{3+}$, Cr^{3+}), MIL-53. *Chem. Commun. (Cambridge, U.K.)* **2003**, 2976−2977.
(71) Liu, Y. Y.; Ju-Lan, Z.; Jian, Z.; Xu, F.; Sun, L. X. Improved Hydrogen Storage in the Modified Metal-Organic Frameworks by Hydrogen Spillover Effect. *Int. J. Hydrogen Energy* **2007**, *32*, 4005−4010.
(72) Salles, F.; Jobic, H.; Maurin, G.; Koza, M. M.; Llewellyn, P. L.; Devic, T.; Serre, C.; Ferey, G. Experimental Evidence Supported by Simulations of a Very High H_2 Diffusion in Metal Organic Framework Materials. *Phys. Rev. Lett.* **2008**, *100*, 245901.
(73) Salles, F.; Kolokolov, D. I.; Jobic, H.; Maurin, G.; Llewellyn, P. L.; Devic, T.; Serre, C.; Ferey, G. Adsorption and Diffusion of H_2 in the MOF Type Systems MIL-47(V) and MIL-53(Cr): A Combination of Microcalorimetry and QENS Experiments with Molecular Simulations. *J. Phys. Chem. C* **2009**, *113*, 7802−7812.
(74) Horcajada, P.; Serre, C.; Maurin, G.; Ramsahye, N. A.; Balas, F.; Vallet-Regi, M.; Sebban, M.; Taulelle, F.; Ferey, G. Flexible Porous Metal-Organic Frameworks for a Controlled Drug Delivery. *J. Am. Chem. Soc.* **2008**, *130*, 6774−6780.
(75) Millange, F.; Serre, C.; Guillou, N.; Ferey, G.; Walton, R. I. Structural Effects of Solvents on the Breathing of Metal-Organic Frameworks: An In Situ Diffraction Study. *Angew. Chem., Int. Ed.* **2008**, *47*, 4100−4105.
(76) Salles, F.; Bourrelly, S.; Jobic, H.; Devic, T.; Guillerm, V.; Llewellyn, P.; Serre, C.; Ferey, G.; Maurin, G. Molecular Insight into the Adsorption and Diffusion of Water in the Versatile Hydrophilic/Hydrophobic Flexible MIL-53(Cr) MOF. *J. Phys. Chem. C* **2011**, *115*, 10764−10776.
(77) Duan, L.; Dong, X.; Wu, Y.; Li, H.; Wang, L.; Song, L. Adsorption and Diffusion Properties of Xylene Isomers and Ethylbenzene in Metal-Organic Framework MIL-53(Al). *J. Porous Mater.* **2013**, *20*, 431−440.
(78) Mulder, F. M.; Assfour, B.; Huot, J.; Dingemans, T. J.; Wagemaker, M.; Ramirez-Cuesta, A. J. Hydrogen in the Metal−Organic Framework Cr MIL-53. *J. Phys. Chem. C* **2010**, *114*, 10648−10655.
(79) Copley, J. R. D.; Cook, J. C. The Disk Chopper Spectrometer at NIST: A New Instrument for Quasielastic Neutron Scattering Studies. *Chem. Phys.* **2003**, *292*, 477−485.
(80) Coelho, A. *TOPAS-Academic* 4.1; Coelho Software: Brisbane, 2007.
(81) Stephens, P. W. Phenomenological Model of Anisotropic Peak Broadening in Powder Diffraction. *J. Appl. Crystallogr.* **1999**, *32*, 281−289.
(82) Azuah, R. T.; Kneller, L. R.; Qiu, Y.; Tregenna-Piggott, P. L. W.; Brown, C. M.; Copley, J. R. D.; Dimeo, R. M. DAVE: A Comprehensive Software Suite for the Reduction, Visualization, and Analysis of Low Energy Neutron Spectroscopic Data. *J. Res. Natl. Inst. Stand. Technol.* **2009**, *114*, 341−358.
(83) Brown, C. M.; Liu, Y.; Yildirim, T.; Peterson, V. K.; Kepert, C. J. Hydrogen Adsorption in HKUST-1: A Combined Inelastic Neutron Scattering and First-Principles Study. *Nanotechnology* **2009**, *20*, 204025.
(84) Haas, O. E.; Simon, J. M.; Kjelstrup, S.; Ramstad, A. L.; Fouquet, P. Quasi-Elastic Neutron Scattering Investigation of the Hydrogen Surface Self-Diffusion on Polymer Electrolyte Membrane Fuel Cell Catalyst Support. *J. Phys. Chem. C* **2008**, *112*, 3121−3125.
(85) Yang, Y.; Brown, C. M.; Zhao, C.; Chaffee, A. L.; Nick, B.; Zhao, D.; Webley, P. A.; Schalch, J.; Simmons, J. M.; Liu, Y.; et al. Micro-Channel Development and Hydrogen Adsorption Properties in Templated Microporous Carbons Containing Platinum Nanoparticles. *Carbon* **2011**, *49*, 1305−1317.
(86) Egelstaff, P. A. *An Introduction to the Liquid State*. Academic Press: New York, 1967.
(87) Jobic, H.; Hahn, K.; Kärger, J.; Bée, M.; Tuel, A.; Noack, M.; Girnus, I.; Kearley, G. J. Unidirectional and Single-File Diffusion of Molecules in One-Dimensional Channel Systems. A Quasi-Elastic Neutron Scattering Study. *J. Phys. Chem. B* **1997**, *101*, 5834−5841.